

Parallel Nanoshaping of Brittle Semiconductor Nanowires for Strained Electronics

Yaowu Hu,^{†,‡} Ji Li,^{†,‡} Jifa Tian,^{†,§} Yi Xuan,[‡] Biwei Deng,^{†,‡} Kelly L. McNear,^{||} Daw Gen Lim,[#] Yong Chen,[†] Chen Yang,^{||,⊥} and Gary J. Cheng^{*,†,‡,§,⊥}

[†]School of Industrial Engineering, Purdue University, West Lafayette, Indiana 47907, United States

[‡]Birck Nanotechnology Center, Purdue University, West Lafayette, Indiana 47907, United States

[§]School of Mechanical Engineering, Purdue University, West Lafayette, Indiana 47907, United States

^{||}Department of Chemistry, Purdue University, West Lafayette, Indiana 47907, United States

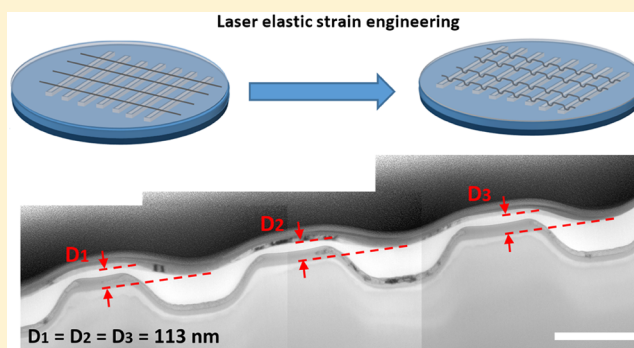
[⊥]Department of Physics, Purdue University, West Lafayette, Indiana 47907, United States

[#]School of Materials Engineering, Purdue University, West Lafayette, Indiana 47907, United States

S Supporting Information

ABSTRACT: Semiconductor nanowires (SCNWs) provide a unique tunability of electro-optical property than their bulk counterparts (e.g., polycrystalline thin films) due to size effects. Nanoscale straining of SCNWs is desirable to enable new ways to tune the properties of SCNWs, such as electronic transport, band structure, and quantum properties. However, there are two bottlenecks to prevent the real applications of straining engineering of SCNWs: strainability and scalability. Unlike metallic nanowires which are highly flexible and mechanically robust for parallel shaping, SCNWs are brittle in nature and could easily break at strains slightly higher than their elastic limits. In addition, the ability to generate nanoshaping in large scale is limited with the current technologies, such as the straining of nanowires with sophisticated manipulators, nanocombing NWs with U-shaped trenches, or buckling NWs with prestretched elastic substrates, which are incompatible with semiconductor technology. Here we present a top-down fabrication methodology to achieve large scale nanoshaping of SCNWs in parallel with tunable elastic strains. This method utilizes nanosecond pulsed laser to generate shock pressure and conformably deform the SCNWs onto 3D-nanostructured silicon substrates in a scalable and ultrafast manner. A polymer dielectric nanolayer is integrated in the process for cushioning the high strain-rate deformation, suppressing the generation of dislocations or cracks, and providing self-preserving mechanism for elastic strain storage in SCNWs. The elastic strain limits have been studied as functions of laser intensity, dimensions of nanowires, and the geometry of nanomolds. As a result of 3D straining, the inhomogeneous elastic strains in GeNWs result in notable Raman peak shifts and broadening, which bring more tunability of the electrical–optical property in SCNWs than traditional strain engineering. We have achieved the first 3D nanostraining enhanced germanium field-effect transistors from GeNWs. Due to laser shock induced straining effect, a more than 2-fold hole mobility enhancement and a 120% transconductance enhancement are obtained from the fabricated back-gated field effect transistors. The presented nanoshaping of SCNWs provide new ways to manipulate nanomaterials with tunable electrical–optical properties and open up many opportunities for nanoelectronics, the nanoelectrical–mechanical system, and quantum devices.

KEYWORDS: Laser shock, germanium nanowires, nanoshaping, elastic strain



Semiconductor nanowires (SCNWs) have unique electrical and optical properties. With the booming demand for increased packaging density and enhanced functionality of nanodevices, SCNWs are deemed as potential candidates as nanoscale building blocks for numerous applications in electronic, electromechanical, photovoltaic, optical, and optoelectronic devices.^{1–8} The physical properties of SCNWs could be effectively tuned through composition modulation^{9,10} or by diameter variation.¹¹ Elastic strain engineering, as an alternative and reversible approach, has attracted intense research interest

to modulate electronic structures of SCNWs and their carrier dynamics. It has been demonstrated that SCNWs can sustain much larger strains than their bulk counterparts, due to increased mechanical strength with less defects and a larger surface/volume ratio,^{12,13} promising the feasibility of strain

Received: August 10, 2016

Revised: November 3, 2016

Published: November 6, 2016

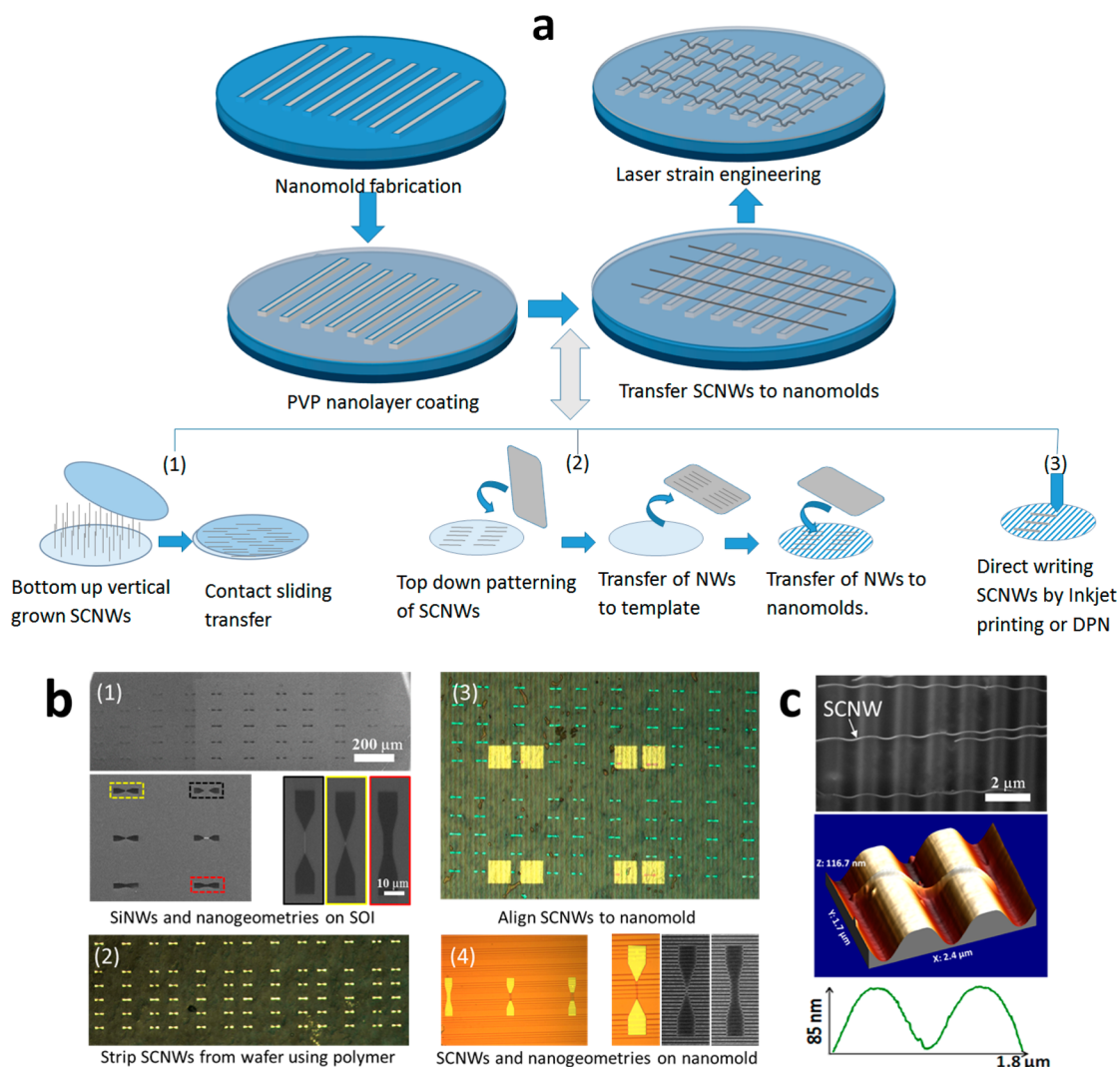


Figure 1. (a) Schematic diagram showing the process flow for laser shock elastic straining of brittle semiconductor nanowires: SiO₂/Si trenches defined by electron-beam lithography, polymer (PVP) cushion coating, transfer of SCNWs to nanomolds by (1) contact printing, (2) transfer printing, and (3) direct writing, and finally nanoshaping of SCNWs by laser shock. (b) Images of (1) SiNWs fabricated on SOI wafer, (2) striped SCNWs on sacrificial polymer, (3) aligned SCNWs, and (4) transferred of SiNWs on nanomolds after removing polymer. (c) Image after nanoshaping GeNWs by LSES and AFM image of a nanoshaped GeNW.

engineering. For example, strained silicon technology has been adopted to boost transistor performance through mobility enhancement.¹⁴ Germanium, an indirect band gap material, can be band gap engineered to a direct band gap of 0.34 eV at 4.2% longitudinal tensile strain,¹⁵ which greatly impacts on the luminescence behavior¹⁶ and lasing action.¹⁷ Enhanced electronic mobility via strain engineering would pave the way for germanium nanowires (GeNWs) to be employed as a promising material for the channels in complementary metal–oxide–semiconductor (CMOS) devices and flexible electronics.

The straining technique has been limited for a long time to lattice mismatch which has several challenges including high density of defects, strain relaxation, and differences of doping diffusion properties.¹⁴ Alternative methods developed in recent years, such as bending with an AFM tip or a manipulator,^{13,18,19} stretching in sophisticated micromechanical straining module²⁰ or etched nanobridges,¹⁹ and buckling through a prestrained elastic substrates such as PDMS,^{21,22} are beneficial for understanding the strain-induced physical and electrical property changes. However, these methods are difficult to be

implemented for practical applications in semiconductor technology, given the fact that they are either inefficient to manufacture on a large scale due to the one-by-one deformation nature, or incapable of integrating reliable electrodes and gating for the fabrication of transistors. A recently developed nanocombing method^{23–25} enables a parallel deterministic assembly of kinked nanowires but is limited to water gating. It is, therefore, imperative to develop a CMOS-compatible approach to controllably deform chemically synthesized SCNWs in a scalable manner, thereby opening the potential to practically implement strain engineered physical properties.

To realize elastic straining of SCNWs, it is desirable that (a) the strain level should be tunable and dislocations or cracks should be avoided; (b) the elastic strain needs to be self-preserved after processing; and (c) the strained SCNWs need to be compatible with silicon technology and sit on substrates with reliable gate modulations. In this Letter, we report on the exploitation of a laser ablation based approach with a predefined nanomold for guided elastic straining, which

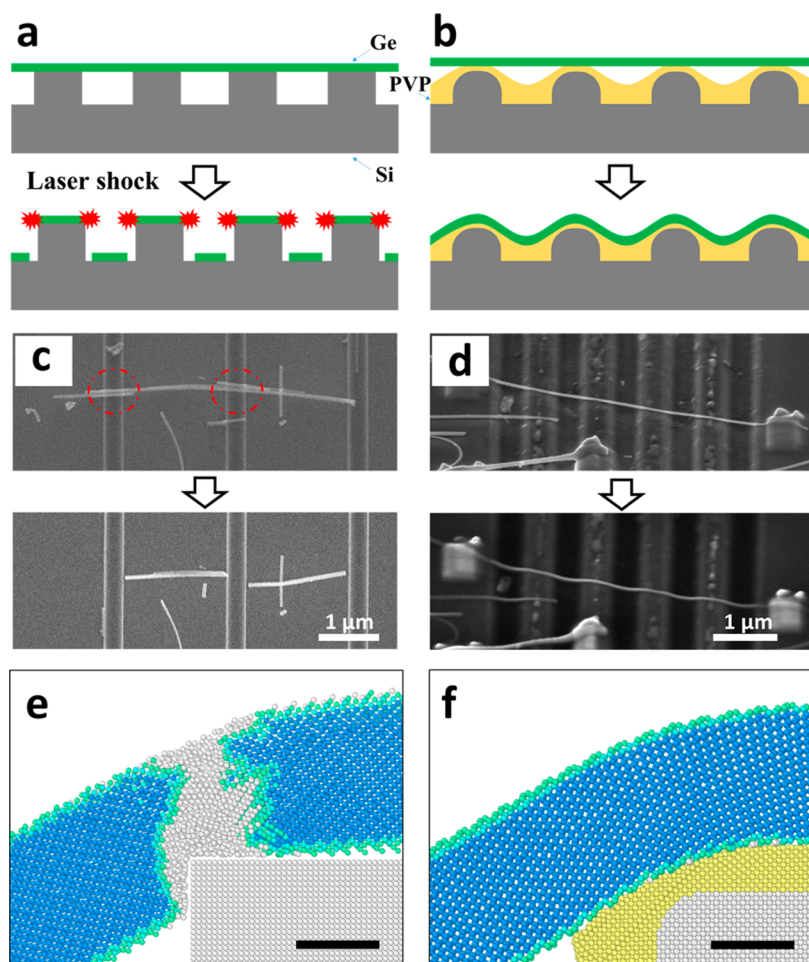


Figure 2. (a) Schematic of GeNWs failures at geometrical sharp corners of silicon mold. (b) Schematic of LSES of GeNWs with smoothed mold corners. Panels c and d are corresponding SEM images of a and b, respectively. (e) Molecular dynamics simulations of c, showing amorphization of GeNW (white area) at sharp corners due to stress concentration. (f) MD simulation of deformation with self-smoothed mold corner by applying deformable materials as cushion (PVP). Scale bars for: (c–d) 1 μm , (e–f) 3 nm.

meets these key requirements. In previous studies, laser shock has been demonstrated to achieve shaping of metal thin film and nanomaterials,^{26–32} with the introduction of high-density dislocations, plastic flow, and defects. However, unlike metallic components which are highly flexible and mechanically robust, SCNWs are brittle in nature and could easily break at strains slightly higher than their limits. The application of laser shock as an ultrafast approach for parallel shaping of SCNWs has never been exploited.

Laser Shock Elastic Straining of Brittle Semiconductor Nanowires. To solve these problems and tackle the present limitations, we develop a laser shock elastic straining (LSES) approach which includes four key steps (Figure 1a). First, nanoscale-channels on Si wafer are fabricated by electron-beam lithography or focused ion beam (FIB) milling. Thermal annealed SiO_2 serves as back-gate dielectric for field effect transistors (FET). Second, a thin layer of insulating polymer is deposited on the nanostructured silicon wafer through dip/spin coating and cross-linked by thermal annealing. Polyvinylpyrrolidone (PVP), a polymer which has been demonstrated to be a high-performance gate dielectric^{33,34} with dielectric constant³⁵ similar to SiO_2 , is used in this study to serve as cushion of nanowire shaping and elastic strain preserver. Third, SCNWs (germanium—GeNW or silicon—SiNW) are grown by bottom-up vapor deposition or top-down lithography and

then transferred onto the mold surface by contact sliding³⁶ (Figure 1a(1)), transfer printing (Figure 1a(2)), or direct printing process³⁷ (Figure 1a(3)). As shown in Figure 1b, the SiNWs are fabricated by e-beam lithography (EBL) of silicon-on-insulator (SOI) wafer followed with dry etching Si layer and lift-off. The SiNWs were then transfer printed onto the nanomold surface. The GeNWs are grown by CVD and transferred on to the nanomolds by contact sliding. Finally, a nanosecond laser is used to generate shock wave to deform the SCNWs, defined either through bottom-up growth or top-down lithography, into the nanomolds conformally (see Materials and Methods in the Supporting Information).

Our approach yields ultrafast elastic straining of brittle SCNWs on silicon substrates. The GeNWs are deformed conformally onto the nanomolds by laser shock elastic straining (LSES) (see Figure 1c). No SCNWs are lost after LSES, giving a shaping yield of 100% for the GeNWs investigated (Figure S1 and S2). During the LSES, an intense pressure is exerted uniformly on the nanowires, which deforms thousands of nanowires into the mold cavities in parallel (Figure S3). The application of LSES does not differentiate between bottom-up and top-down NWs or nanogeometries: once the NWs are transferred onto the target substrate, LSES could yield effective straining (Figure S4). The shock pressure can be controlled by the laser intensity, confinement, and ablative coating. The

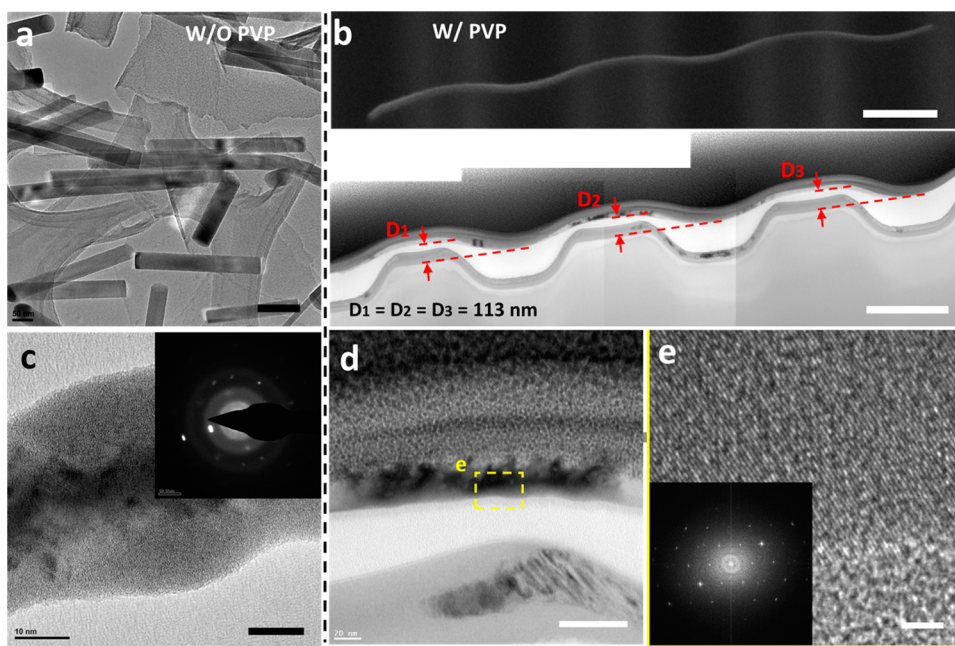


Figure 3. (a) TEM images of fragmented GeNWs after shocking without PVP. (b) Tilted-view SEM image of LSES of GeNW (upper), and TEM cross-sectional view of the GeNW by FIB milling showing identical deformation depths across three trench gaps (lower). Scale bars: 1 μm and 500 nm. (c) TEM image of individual GeNW by laser shock without PVP. Inset is the diffraction pattern showing amorphization of GeNW. (d–e) HRTEM images of the GeNW at the trench corners showing elastic deformation of GeNW with LSES. Inserted is the diffraction pattern. Scale bars: (a) 100 nm, (b) 1 μm and 500 nm for upper and lower images, (c) 10 nm, (d) 50 nm, and (e) 2 nm.

nanowires can be considered as free beams at suspending parts and are pinned at the bar sections by the high pressure. There is no significant sliding or turning of the nanowires on the mold surface. Highly reliable controlled deformation in the elastic region is critical and is realized by smooth transitions of mold geometries and the polymer cushion. As the nanowires gain the momentum from laser shock and get deformed against the polymer thin layer on silicon mold, viscoplastic deformation of the polymer consumes excessive shock energy and eliminates stress concentration by avoiding point contacts between the brittle SCNWs with the substrate. It should be noted that the laser shock process takes place within tens of nanoseconds, yielding an ultrahigh strain rate not achievable in traditional methods. This would inhibit brittle cracking triggered by random imperfections on the nanowire surface in the case of low strain rates.³⁸ The advantage of LSES also lies in the fact that the elastically deformed SCNWs, which normally tends to relax to the unstrained state after unloading, is self-anchored through van der Waals interactions between SCNWs and the polymer thin layer, while state-of-the-art strained electrical devices based on chemically synthesized SCNWs provide no mechanism to maintain the elastic deformation after relieving the external loads.

Interaction between the SCNWs and 3D Nanostructured Substrates. The deformation behavior of the shocked SCNWs in LSES strongly depends on their contacts with mold surfaces. When directly shocking SCNWs on silicon or silicon dioxide surfaces, their “hard” contacts, especially those at the structural edges, can result in failures. Silicon molds fabricated through wet/dry etching are typically with atomically sharp edges, which would result in giant stress concentrations and damages to the brittle nanowires. Although the laser pressure used is less than 1 GPa, which is lower than the strength of the GeNWs, the stress concentration effect at the point or line contacts, results in much larger localized stress,

irreversible plastic deformations (amorphization) and shear-stress induced cracks, as shown schematically in Figure 2a, demonstrated experimentally in Figure 2c and numerically in Figure 2e and Figures S5 and S6. Highly localized elastic strains in a nanowire before its failure, if any, are difficult to control. The strains are relaxed once the SCNWs are broken. In the LSES approach, we tackle this problem by employing polymer cushioning and mold edge rounding. The deformation interlayer between GeNWs and the “hard” silicon substrate; e.g., the polymer cushion creates an opportunity for soft landing of the GeNWs (Figure 2b). It provides a self-smoothing mechanism of the sharp geometries and could dynamically accommodate stress distributions. We also fabricate rounded edges by appropriate adjusting electron/ion beam parameters and thermal annealing. A wavy GeNW strained on a round trench shown in Figure 2d and f could be obtained after laser shock. By pinning the nanowire with deposited metals, we demonstrate that the process is not due to sliding of the nanowire at mold surface, and an obvious length elongation is observed.

To further demonstrate the elastic straining of GeNWs by LSES, high-resolution transmission electron microscopy (HRTEM) was carried out on the cross section achieved via FIB milling of a strained GeNW petrified by PVP. Laser shock of GeNWs without PVP cushion was found to result in fragmentation of brittle nanowires (Figure 3a) or large plastic deformation due to dislocation-initiated amorphization during ultrahigh strain rate deformation (Figure 3c). When GeNWs were shocked on PVP, the deformation behavior is elastic (Figure 3b–e). We found that all of the deformation depths of the 3- μm -long GeNW on the three gaps, namely, D_1 , D_2 , and D_3 (defined as the vertical distances between the trench center and the gap center), are equal to 113 nm. The equivalence of the depths is thought-provoking. As the nanowire is not pinned by any external forces, the boundary conditions for

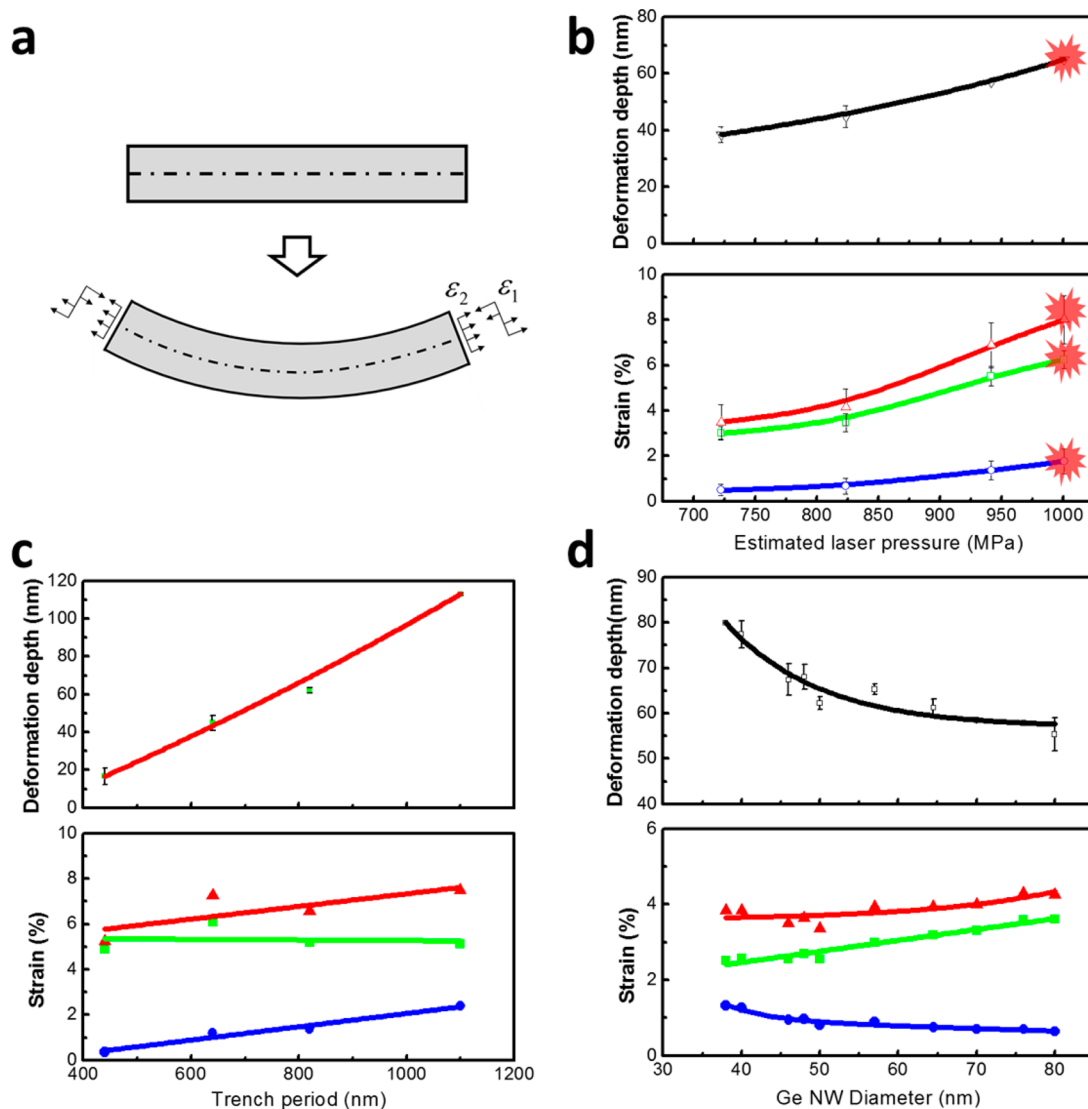


Figure 4. (a) Schematic of uniaxial and bending strain components introduced by laser shock. (b–c) Trends showing the dependence of deformation depth and total average strain as well as its components with (b) estimated laser pressure (trench width: 300 nm and GeNWs diameter: 60 nm), (c) trench width (laser pressure: 940 MPa; GeNWs diameter: 60 nm), and (d) GeNW diameter (laser pressure: 940 MPa and trench width: 300 nm).

deformations in the three gaps are different. However, the equivalence of depths suggests that the process is self-pinned, and no significant sliding occurs between adjacent gaps. Otherwise the less constrained deformation in D3 would be larger than the other two. The self-pinning effect is due to the deformation of the aluminum flyer and its interactions (including frictions) with GeNWs and PVP cushion, as well as the ultrafast processing nature which petrifies the morphology instantaneously. Based on the observed nanowire morphology, a tensile bending strain of 4.2% and a uniaxial strain of 2.4% could be calculated, giving a maximum total strain of 6.6%, which are the highest strain levels to date in GeNWs based on a top-down parallel straining approach. At trench corners, no dislocations or amorphization could be observed on the GeNW, as shown in Figure 3d–e, which agrees with our molecular dynamics simulations in Figure 2f and demonstrates the elastic straining nature of LSES. We also carried out an experiment to investigate the strain recovery by dissolving the polymer in alcohol to release the strain; straightening of the shaped GeNWs with metal pinned at

their two ends was observed (Figure S7). The elastic straining of LSES is thus benefited from the smooth silicon structure corners and also the cushion performance of PVP, which avoids stress concentrations during nanoshaping of GeNWs.

Elastic Strain Limit of GeNWs during LSES. The LSES straining strategy generates both uniaxial tensile strain, which is controlled by mold geometries, and bending strain which varies with nanowire diameters. As shown in Figure 4a, when the nanowires break at the center of trench gaps due to combined bending and uniaxial tension stress, the maximum strains are achieved. The bending strain is estimated by³⁹

$$\epsilon_1 = r/(r + R) \quad (1)$$

where r and R are the nanowire radius and the radius of bending curvature, respectively. The axial strain is determined by

$$\epsilon_2 = \ln(L/L_0) \quad (2)$$

where L_0 and L are the original and deformed segment length of GeNWs along the cavity in trench mold. The total strain

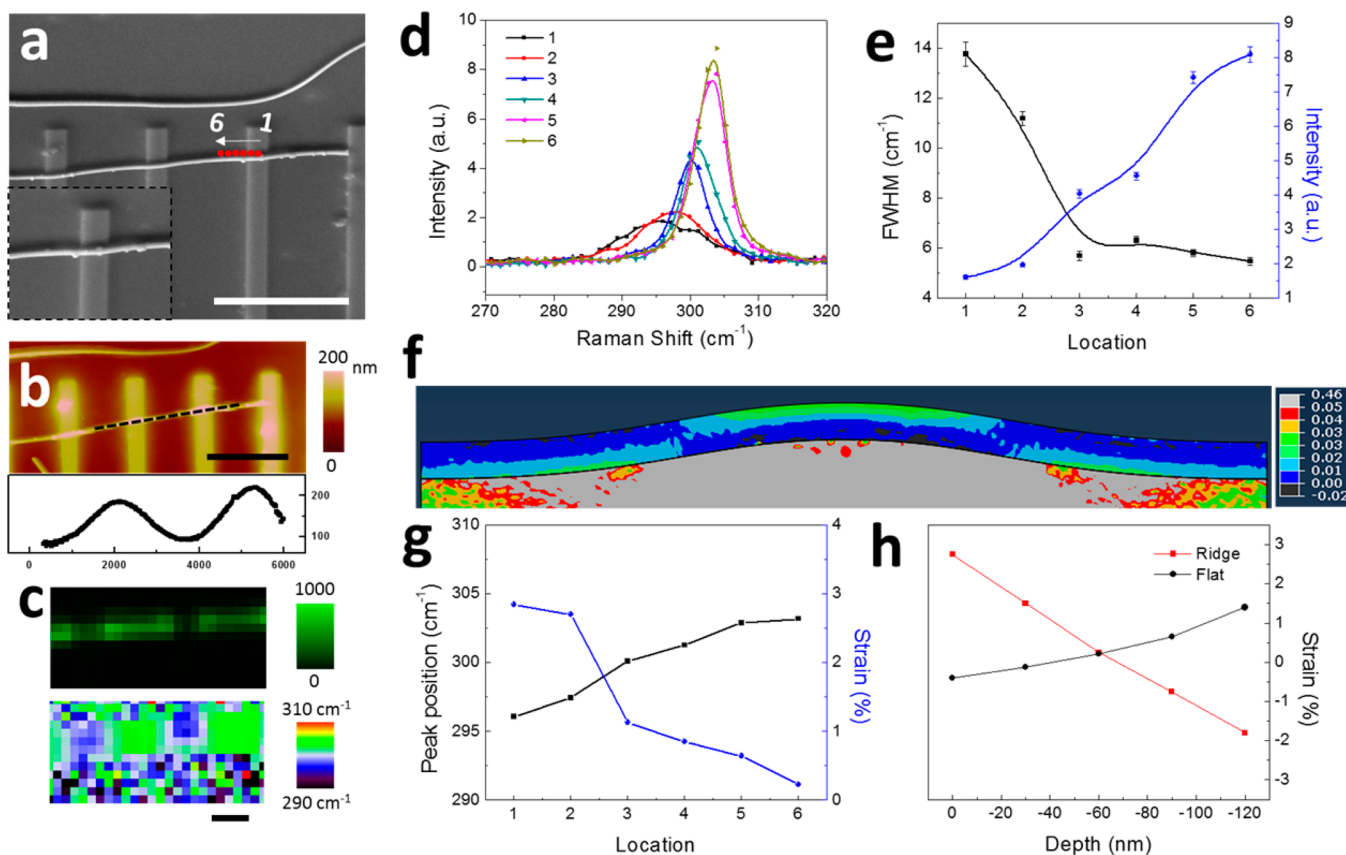


Figure 5. Raman spectroscopy characterization of strain distribution in shaped GeNWs. (a) SEM image of the GeNW investigated. (b) AFM height (upper) and line profile (lower) measurements of the nanowire. (c) Measured Raman intensity (upper) and peak position (lower) mapping. (d) Raman spectra from 270 to 320 cm^{-1} . The positions are indicated in panel a. (e) Measured Ge peak fwhm and intensities. (f) Simulated strain fields of the GeNW by FEM. (g) Plot of Raman peak shifts and calculated strains. (h) Strain variations along depth directions. Scale bars: (a) 4 μm , (b) 3 μm , and (c) 1 μm .

could be calculated by adding the two components of strain. As the laser beam size is in millimeters and the beam position can be controlled by a beam scanner, the laser shock nanoshaping process is a scalable technique. Depending on the mold area and the coverage density of the GeNWs, hundreds and thousands of nanowires can be nanoshaped simultaneously with a laser pulse.

We further carried out various parametric studies to validate and establish LSES of GeNWs in particular and for SCNWs in general. Experimental parameters such as (a) laser pressure, (b) trench width, and (c) GeNW diameter are varied to investigate their influences on deformation depths and straining levels, as shown in Figure 4b–d. The laser shock pressure values are estimated by Fabbro's model^{40,41} and can be controlled by adjusting the laser intensity. It should be noted that the shock pressure, which involves dynamic responses of nanosystems, is different from a hydrostatic pressure, and its actual value applied on the nanowires is slightly smaller than the reported laser shock pressure due to the attenuation in the aluminum foil. Experiments were carried out until the fracture point of GeNWs. It is observed that deformation depth and average strain increase almost linearly, with the increase in laser shock pressure as shown in Figure 4b before the nanowires attain a fracture. Contributions of both bending strain (strain 1) and axial strain (strain 2) to the total strain are also shown in Figure 4b. The bending curvature has been observed to decrease with increasing pressure. The smallest curvature attained before fracture commences for a 60 nm nanowire is approximately 450

nm. Figure 4c and d represents the effect of trench width and GeNWs diameter on strains under constant pressure. As can be observed from Figure 4c, the increase in the trench width induces higher bending and axial strains in the system. Figure 4d shows the dependence of deformation depth and strain on the nanowire diameter under constant shock pressure. Interestingly, the increase in bending strain is balanced by the decrease in the axial strain. The bending strain increases with the diameter, while the uniaxial one decreases, resulting in a constant total strain over the diameter from 30 to 80 nm.

Inhomogeneous Elastic Strains in GeNWs after 3D Nanoshaping. To further confirm that the elastic nature of LSES and shed light on the strain distributions, spatially resolved Raman spectroscopy is employed with circularly polarized 532 nm excitation, a 100 \times objective lens with numerical aperture NA = 0.85, and a fiber coupled grating spectrometer (2400 lines/mm). The laser intensity was kept sufficiently low to avoid heating effect. Arrays of far-isolated ridges are designed for better strain visualization. The surface morphology of the nanowire investigated is shown in Figure 5a,b. The obtained Raman spectra around the shaped nanowire, including the Ge peak intensities and peak positions, are shown in Figure 5c,d. The silicon peaks are located at 520.1 cm^{-1} for all obtained spectra (Figure S8), while the Ge peaks are continuously blue-shifted from the ridge top to the trench center (see Figure 5d), indicating a spatially varied tensile strains. The Ge peak on the ridge is significantly broadened and has a decreased intensity (Figure 5e), compared to the

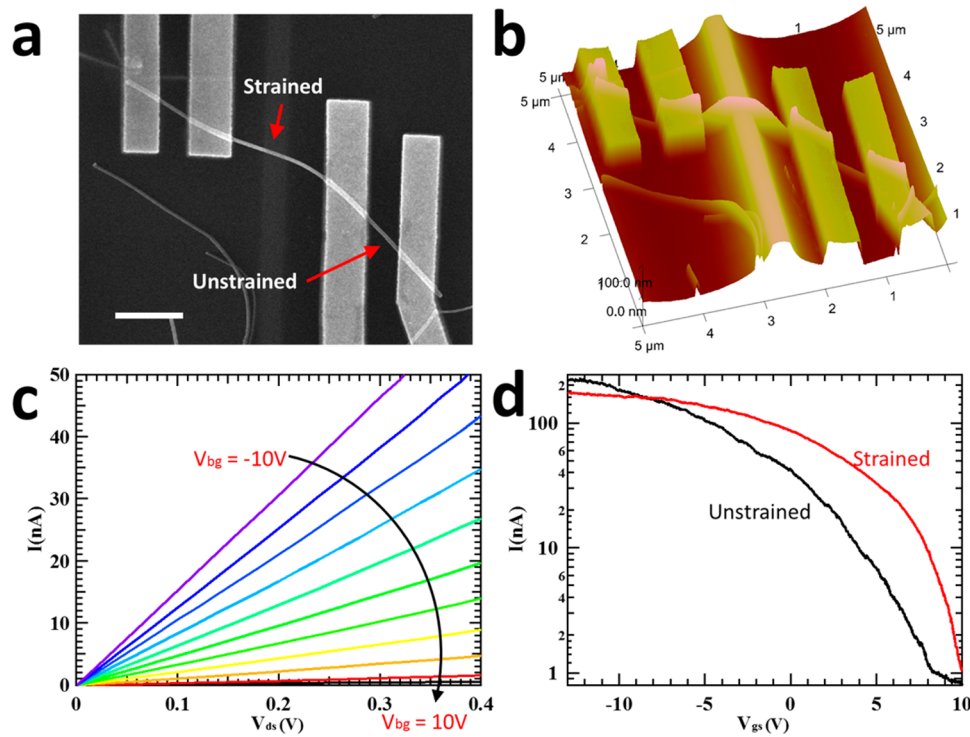


Figure 6. (a) SEM and (b) AFM imaging of the fabricated laser shock strained GeNW device. Scale bar: 1 μm . (c) Output characteristics and (d) transfer characteristics of the GeNW device. The strained area is at the proximity of the trench, while the rest is unstrained. The channel length of the strained area is 1.4 μm , while that of the unstrained area is 600 nm.

nonshaped nanowires. The observed peak shifts are compared with strain fields obtained through finite element modeling (FEM), as shown in Figure 5f. The maximum peak shift of 7.1 cm^{-1} in this nanowire corresponds to an average tensile strain of 2.4% along [111] crystallographic directions within the circularly polarized laser spot.^{42–44} The peak is also significantly broadened due to strain variations within the probed area, in both lateral and depth directions, as shown in Figure 5g–h. Based on the AFM profiling and FEM modeling, we calculate the elastic strain at the ridge to be 2.8%, which agrees well with the experimental data. Similar results are obtained on other strained GeNWs (Figure S9), demonstrating the elastic straining nature of the described LSES approach.

Laser Shock Induced Straining Effect on FET Device Performance. Unlike traditional straining techniques based on lattice mismatch, or polymer substrates stretching, LSES is versatile for applying controllable strains up to the strain limit of the material and being compatible with current semiconductor technology (Figure S10). To shine light on the laser shock induced straining effect on FET device performance, the transfer and output characteristics of the strained and unstrained areas on the same NW are compared. As shown in Figure 6, a GeNW is placed across a bump of a periodic trench structure, which generates bending strain of the NW at its proximity. The bump feature is adopted here in accordance with the Raman measurement in Figure 5 which, due to system resolution limits, has periodic bumps far from each other to achieve the noticeable peak shifts. The strain distributions are thus slightly different from but are fundamentally the same with the ones in Figure 4 for the characterization of mechanical properties. The strains on the top of the nanowires are tensile in the present case, as shown in Figure 5f. An alternative option of the present design is increasing the bump width to make

isolated trenches (into the surface), changing the strain on the top surface to compressive. However, this option increases the writing time for E-beam lithography when hydrogen silsesquioxane (HSQ) is used. The field-effect mobility could be calculated by

$$\mu = \frac{dI_{DS}}{dV_{GS}} \times \frac{L^2}{C_e} \times \frac{1}{V_{DS}} \quad (4)$$

where I_{DS} is the source–drain current, V_{GS} the gate voltage, L the channel length, and V_{DS} is the source–drain voltage. Since PVP has approximately the same dielectric constant³⁵ with SiO_2 , C_e the effect gate capacitance is given by

$$C_e = \frac{2\pi\epsilon_0\epsilon L}{\cosh^{-1}\left(\frac{R+t_e}{R}\right)} \quad (5)$$

where t_e and ϵ are the effective thickness and the dielectric constant, respectively. The diameter of the nanowire at both strained and unstrained parts is measured five times with high-resolution SEM imaging to yield an average value of 60 nm and standard variation of 3 nm.

$t_e \approx t_{\text{ox}} + t_p$, where t_{ox} and t_p are the thickness of SiO_2 and PVP, respectively. The unstrained part has $t_{\text{ox}} = 90\text{ nm}$, $t_p = 125\text{ nm}$; for the strained part has $t_{\text{ox}} = 240\text{ nm}$, $t_p = 100\text{ nm}$. The mobility enhancement is determined by

$$\frac{\mu_s}{\mu_{\text{us}}} = \left(\frac{dI_{DS}}{dV_{GS}}\right)_s \times \frac{L_s}{L_{\text{us}}} \times \frac{(C_e)_{\text{us}}}{(C_e)_s} \quad (6)$$

The strain results in a 120% enhanced transconductance and 238% enhanced field-effect hole mobility (see Supporting Information), due to modification of the effective masses.⁴⁵ The

device on/off ratio is also found to be decreased from 2.77×10^2 to 1.76×10^2 , agreeing with the band gap shrinkage under the presence of both tensile and compressive strains. A similar phenomenon was found in several other nanowires from the same batch and same nanomold after laser straining, with a mobility increase by 230–260%, and a transconductance increase by 120–150%. The on/off ratio was decreased by about 30–40%. It should be noted that these values could vary when different mold structural dimensions and laser parameters are applied, as they effectively tune the three-dimensional strains and strain gradients. As the thicknesses of gate dielectrics for the strained and unstrained devices are different, the device performance could be further boosted by adopting conformal top gating. In principle, the strain fields of the SCNWs could be designed by adjusting laser parameters and mold geometries, yielding tunable band structure engineering, the details of which are beyond the scope of the current work and leave large room for future device performance optimization.

In conclusion, we have demonstrated for the first time that brittle SCNWs can be nanoshaped at ultrahigh strain rate in an ultrafast and controllable manner. This method utilizes laser-induced shock loading to deform SCNWs onto 3D-nanostructured silicon substrates with a cushioning polymer dielectric nanolayer, resulting in the storage of elastic strains in SCNWs without dislocations or cracks. The elastic straining achieved by LSES is self-preserved and CMOS-compatible. We have studied the effects of processing parameters, such as mold geometries (e.g., corner sharpness and trench width), laser pressure, and nanowire diameters, on the deformation behavior and elastic strain limits. The elastic strains of GeNWs are experimentally investigated by spatially resolved Raman spectroscopy and TEM and confirmed by numerical simulations at both atomic and continuum-mechanics scales. The tunable strains resulted in SCNWs can be controlled by the laser intensity, dimensions of nanowires, and geometry of nanomolds. As a result of 3D straining, the inhomogeneous elastic strains in GeNWs results in notable Raman peak shifts and broadening, which bring more tunability of electrical-optical property in SCNWs than traditional strain engineering. Nanowire FETs are fabricated with LSES treated GeNWs, and it is found to yield significantly enhanced hole mobilities and modulated on/off ratios. This laser-based nanoshaping technique is versatile and suitable for variety of semiconductor nanowires and other 1D nanostructures. The findings in this study would potentially bring many breakthroughs in future, as it provides a clean technology for band engineering of SCNWs for large-scale applications.

■ ASSOCIATED CONTENT

Supporting Information

The Supporting Information is available free of charge on the ACS Publications website at DOI: [10.1021/acs.nanolett.6b03366](https://doi.org/10.1021/acs.nanolett.6b03366).

Materials and methods, AFM images of the same GeNWs before and after laser shock, MD simulation of shear stress concentration at sharp mold corners, cycled shaping with laser shock and polymer dissolving, Raman spectra of GeNWs at germanium peaks and silicon peaks, fabricated strained GeNW FET with a large on/off ratio, and methods for mobility calculations (PDF)

■ AUTHOR INFORMATION

Corresponding Author

*Phone: 765 49-45436, e-mail: gjcheng@purdue.edu.

ORCID

Jifa Tian: 0000-0003-2921-470X

Gary J. Cheng: 0000-0002-1184-2946

Notes

The authors declare no competing financial interest.

■ ACKNOWLEDGMENTS

We sincerely thank the US National Science Foundation through CMMI (grant number 1538360) for financial support and the Purdue Office of Vice President for Research through an incentive research grant.

■ REFERENCES

- (1) Ionescu, A. M. Electronic Devices: Nanowire Transistors Made Easy. *Nat. Nanotechnol.* **2010**, *5*, 178–179.
- (2) Xu, S.; Qin, Y.; Xu, C.; Wei, Y.; Yang, R.; Wang, Z. L. Self-Powered Nanowire Devices. *Nat. Nanotechnol.* **2010**, *5*, 366–373.
- (3) Ju, S.; Facchetti, A.; Xuan, Y.; Liu, J.; Ishikawa, F.; Ye, P.; Zhou, C.; Marks, T. J.; Janes, D. B. Fabrication of Fully Transparent Nanowire Transistors for Transparent and Flexible Electronics. *Nat. Nanotechnol.* **2007**, *2*, 378–384.
- (4) Husain, A.; Hone, J.; Postma, H. W. C.; Huang, X. M. H.; Drake, T.; Barbic, M.; Scherer, A.; Roukes, M. L. Nanowire-Based Very-High-Frequency Electromechanical Resonator. *Appl. Phys. Lett.* **2003**, *83*, 1240–1242.
- (5) Adachi, M. M.; Anantram, M. P.; Karim, K. S. Core-Shell Silicon Nanowire Solar Cells. *Sci. Rep.* **2013**, *3*, 2–7.
- (6) Cao, L.; White, J. S.; Park, J.-S.; Schuller, J. A.; Clemens, B. M.; Brongersma, M. L. Engineering Light Absorption in Semiconductor Nanowire Devices. *Nat. Mater.* **2009**, *8*, 643–647.
- (7) Babinec, T. M.; Hausmann, B. J. M.; Khan, M.; Zhang, Y.; Maze, J. R.; Hemmer, P. R.; Loncar, M. A Diamond Nanowire Single-Photon Source. *Nat. Nanotechnol.* **2010**, *5*, 195–199.
- (8) Li, Y.; Qian, F.; Xiang, J.; Lieber, C. M. Nanowire Electronic and Optoelectronic Devices. *Mater. Today* **2006**, *9*, 18–27.
- (9) Gu, F.; Yang, Z.; Yu, H.; Xu, J.; Wang, P.; Tong, L.; Pan, A. Spatial Bandgap Engineering along Single Alloy Nanowires. *J. Am. Chem. Soc.* **2011**, *133*, 2037–2039.
- (10) Shin, J. C.; Kim, K. H.; Yu, K. J.; Hu, H.; Yin, L.; Ning, C.; Rogers, J. A.; Zuo, J.; Li, X. In X Ga 1- X As Nanowires on Silicon: One-Dimensional Heterogeneous Epitaxy, Bandgap Engineering, and Photovoltaics. *Nano Lett.* **2011**, *11*, 4831–4838.
- (11) Myalitsin, A.; Strelow, C.; Wang, Z.; Li, Z.; Kipp, T.; Mews, A. *ACS Nano* **2011**, *5*, 7920–7927.
- (12) Smith, D. A.; Holmberg, V. C.; Lee, D. C.; Korgel, B. A. Young's Modulus and Size-Dependent Mechanical Quality Factor of Nano-electromechanical Germanium Nanowire Resonators. *J. Phys. Chem. C* **2008**, *112*, 10725–10729.
- (13) Hoffmann, S.; Utke, I.; Moser, B.; Michler, J.; Christiansen, S. H.; Schmidt, V.; Senz, S.; Werner, P.; Gösele, U.; Ballif, C. Measurement of the Bending Strength of Vapor-Liquid-Solid Grown Silicon Nanowires. *Nano Lett.* **2006**, *6*, 622–625.
- (14) Jeong, M. Silicon Device Scaling to the Sub-10-Nm Regime. *Science (Washington, DC, U. S.)* **2004**, *306*, 2057–2060.
- (15) Zhang, F.; Crespi, V. H.; Zhang, P. Prediction That Uniaxial Tension along 111 Produces a Direct Band Gap in Germanium. *Phys. Rev. Lett.* **2009**, *102*, 1–4.
- (16) Audoit, G.; Mhuircheartaigh, É. N.; Lipson, S. M.; Morris, M. A.; Blau, W. J.; Holmes, J. D. Strain Induced Photoluminescence from Silicon and Germanium Nanowire Arrays. *J. Mater. Chem.* **2005**, *15*, 4809.

- (17) Liu, J.; Sun, X.; Camacho-Aguilera, R.; Kimerling, L. C.; Michel, J. Ge-on-Si Laser Operating at Room Temperature. *Opt. Lett.* **2010**, *35*, 679–681.
- (18) Smith, D. A.; Holmberg, V. C.; Korgel, B. A. Flexible Germanium Nanowires: Ideal Strength, Room Temperature Plasticity, and Bendable Semiconductor Fabric. *ACS Nano* **2010**, *4*, 2356–2362.
- (19) Süess, M. J.; Geiger, R.; Minamisawa, R. A.; Schiefler, G.; Frigerio, J.; Chrastina, D.; Isella, G.; Spolenak, R.; Faist, J.; Sigg, H. Analysis of Enhanced Light Emission from Highly Strained Germanium Microbridges. *Nat. Photonics* **2013**, *7*, 466–472.
- (20) Greil, J.; Lugstein, A.; Zeiner, C.; Strasser, G.; Bertagnolli, E. Tuning the Electro-Optical Properties of Germanium Nanowires by Tensile Strain. *Nano Lett.* **2012**, *12*, 6230–6234.
- (21) Ryu, S. Y.; Xiao, J.; Park, W. Il; Son, K. S.; Huang, Y. Y.; Paik, U.; Rogers, J. A. Lateral Buckling Mechanics in Silicon Nanowires on Elastomeric Substrates. *Nano Lett.* **2009**, *9*, 3214–3219.
- (22) Xu, F.; Lu, W.; Zhu, Y. Controlled 3D Buckling of Silicon Nanowires for Stretchable Electronics. *ACS Nano* **2011**, *5*, 672–678.
- (23) Yao, J.; Yan, H.; Lieber, C. M. A Nanoscale Combing Technique for the Large-Scale Assembly of Highly Aligned Nanowires. *Nat. Nanotechnol.* **2013**, *8*, 329–335.
- (24) Yao, J.; Yan, H.; Das, S.; Klemic, J. F.; Ellenbogen, J. C.; Lieber, C. M. Nanowire Nanocomputer as a Finite-State Machine. *Proc. Natl. Acad. Sci. U. S. A.* **2014**, *111*, 2431–2435.
- (25) Zhao, Y.; Yao, J.; Xu, L.; Mankin, M. N.; Zhu, Y.; Wu, H.; Mai, L.; Zhang, Q.; Lieber, C. M. Shape-Controlled Deterministic Assembly of Nanowires. *Nano Lett.* **2016**, *16*, 2644.
- (26) Hu, Y.; Kumar, P.; Xu, R.; Zhao, K.; Cheng, G. J. Ultrafast Direct Fabrication of Flexible Substrate-Supported Designer Plasmonic Nanoarrays. *Nanoscale* **2016**, *8*, 172–182.
- (27) Gao, H.; Hu, Y.; Xuan, Y.; Li, J.; Yang, Y.; Martinez, R. V.; Li, C.; Luo, J.; Qi, M.; Cheng, G. J. Large-Scale Nanoshaping of Ultrasmooth 3D Crystalline Metallic Structures. *Science (Washington, DC, U. S.)* **2014**, *346*, 1352–1356.
- (28) Kumar, P.; Li, J.; Nian, Q.; Hu, Y.; Cheng, G. J. Plasmonic Tuning of Silver Nanowires by Laser Shock Induced Lateral Compression. *Nanoscale* **2013**, *5*, 6311.
- (29) Hu, Y.; Lee, S.; Kumar, P.; Nian, Q.; Wang, W.; Irudayaraj, J. J.; Cheng, G. J. Water Flattens Graphene Wrinkles: Laser Shock Wrapping of Graphene onto Substrate-Supported Crystalline Plasmonic Nanoparticle Arrays. *Nanoscale* **2015**, *7*, 19885.
- (30) Li, J.; Liao, Y.; Suslov, S.; Cheng, G. J. Laser Shock-Based Platform for Controllable Forming of Nanowires. *Nano Lett.* **2012**, *12*, 3224–3230.
- (31) Hu, Y.; Kumar, P.; Xuan, Y.; Deng, B.; Qi, M.; Cheng, G. J. Controlled and Stabilized Light-Matter Interaction in Graphene: Plasmonic Film with Large-Scale 10-Nm Lithography. *Adv. Opt. Mater.* **2016**, DOI: 10.1002/adom.201600201.
- (32) Hu, Y.; Xuan, Y.; Wang, X.; Deng, B.; Saei, M.; Jin, S.; Irudayaraj, J.; Cheng, G. J. Superplastic Forming of Metal Nanostructure Arrays with Ultrafine Gaps. *Adv. Mater.* **2016**, *28*, 1–11.
- (33) Roberts, M. E.; Queraltó, N.; Mannsfeld, S. C. B.; Reinecke, B. N.; Knoll, W.; Bao, Z. Cross-Linked Polymer Gate Dielectric Films for Low-Voltage Organic Transistors. *Chem. Mater.* **2009**, *21*, 2292–2299.
- (34) Klauk, H.; Halik, M.; Zschieschang, U.; Schmid, G.; Radlik, W.; Weber, W. High-Mobility Polymer Gate Dielectric Pentacene Thin Film Transistors. *J. Appl. Phys.* **2002**, *92*, 5259.
- (35) Chen, F. C.; Chu, C. W.; He, J.; Yang, Y.; Lin, J. L. Organic Thin-Film Transistors with Nanocomposite Dielectric Gate Insulator. *Appl. Phys. Lett.* **2004**, *85*, 3295–3297.
- (36) Javey, A.; Nam, S.; Friedman, R. S.; Yan, H.; Lieber, C. M. Layer-by-Layer Assembly of Nanowires for Three-Dimensional, Multifunctional Electronics. *Nano Lett.* **2007**, *7*, 773–777.
- (37) Carlson, A.; Bowen, A. M.; Huang, Y.; Nuzzo, R. G.; Rogers, J. a. Transfer Printing Techniques for Materials Assembly and Micro/nanodevice Fabrication. *Adv. Mater.* **2012**, *24*, 5284–5318.
- (38) Ramachandramoorthy, R.; Gao, W.; Bernal, R.; Espinosa, H. High Strain Rate Tensile Testing of Silver Nanowires: Rate-Dependent Brittle-to-Ductile Transition. *Nano Lett.* **2016**, *16*, 255.
- (39) Zhang, Z.; Han, X. D.; Zhang, Y. F.; Zheng, K.; Zhang, X. N.; Hao, Y. J.; Guo, X. Y.; Yuan, J.; Wang, Z. L. Low-Temperature in Situ Large Strain Plasticity of Ceramic SiC Nanowires and Its Atomic-Scale Mechanism. *Nano Lett.* **2007**, *7*, 452–457.
- (40) Fabbro, R.; Fournier, J.; Ballard, P.; Devaux, D.; Virmont, J. Physical Study of Laser-Produced Plasma in Confined Geometry. *J. Appl. Phys.* **1990**, *68*, 775.
- (41) Devaux, D.; Fabbro, R.; TOLLIER, L.; Bartnicki, E. Generation of Shock Waves by Laser-Induced Plasma in Confined Geometry. *J. Appl. Phys.* **1993**, *74*, 2268–2273.
- (42) Peng, C. Y.; Huang, C. F.; Fu, Y. C.; Yang, Y. H.; Lai, C. Y.; Chang, S. T.; Liu, C. W. Comprehensive Study of the Raman Shifts of Strained Silicon and Germanium. *J. Appl. Phys.* **2009**, *105*, 083537.
- (43) Süess, M. J.; Minamisawa, R. A.; Geiger, R.; Bourdelle, K. K.; Sigg, H.; Spolenak, R. Power-Dependent Raman Analysis of Highly Strained Si Nanobridges. *Nano Lett.* **2014**, *14*, 1249.
- (44) Süess, M. J.; Geiger, R.; Minamisawa, R. a.; Schiefler, G.; Frigerio, J.; Chrastina, D.; Isella, G.; Spolenak, R.; Faist, J.; Sigg, H. Analysis of Enhanced Light Emission from Highly Strained Germanium Microbridges. *Nat. Photonics* **2013**, *7*, 466–472.
- (45) Riddet, C.; Watling, J. R.; Chan, K. H.; Parker, E. H. C.; Whall, T. E.; Leadley, D. R.; Asenov, A. Hole Mobility in Germanium as a Function of Substrate and Channel Orientation, Strain, Doping, and Temperature. *IEEE Trans. Electron Devices* **2012**, *59*, 1878–1884.